https://doi.org/10.5194/egusphere-2025-5252
Preprint. Discussion started: 17 November 2025

Geothermal implications of the lithosphere's thermal structure in northern Pakistan

Muhammad Anees[1, 2], David Hindle[2], Ernesto Meneses Rioseco[1, 2], Jonas Kley[1], Bernd Leiss[1], Mumtaz M. Shah[3], Javed Akhter Qureshi[4]

[1]LIAG Institute for Applied Geophysics, Hannover, Germany
[2]Department of Structural Geology and Geothermics, Geoscience Centre, Georg-August-Universität Göttingen, Germany
[3]Department of Earth Sciences, Quaid-i-Azam University, Islamabad, Pakistan
[4]Department of Geology and Mountain Hazards, Karakoram International University, Gilgit, Pakistan

Correspondence to: Muhammad Anees (muhammad.anees@liag-institut.de)

Abstract. Conventional geothermal resources are typically associated with volcanically active plate boundaries, yet collisional orogens can also sustain elevated heat flow through radiogenic enrichment, crustal thickening, and rapid exhumation. Northern Pakistan, encompassing the Himalaya, Kohistan, and Karakoram terranes, hosts numerous hot springs aligned with major fault zones despite the absence of active volcanism. The origin of this anomalous heat remains debated, reflecting the lack of surface heat flow measurements and limited geophysical constraints on the lithosphere. To address this gap, we apply 1D steady-state, 1D transient, and 2D advective–conductive thermal models to the Nanga Parbat Massif (NPM), Kohistan arc, and Karakoram terrane resulting from translation of heat conduction due to exhumation of blocks. Steady-state results show strong dependence of geotherms on crustal radiogenic heat production (RHP): in the NPM, upper-crustal enrichment (4–5 μWm^{-3}) yields surface heat flow of 85–120 mW m^{-2}, whereas Kohistan produces lower values (50–85 mW m^{-2}) due to its mafic-dominated crust. Karakoram yields intermediate heat flow (65–103 mW m^{-2}), with RHP concentrated in the batholith and metamorphic complexes. ID transient exhumation models demonstrate that uplift rates of 2–3 mm y^{-1} in the NPM can further amplify geotherms, producing surface heat flow up to 220–250 mW m^{-2} and inverting deep geotherms at 20 km when RHP is high. Two-dimensional thermal simulations capture the combined effects of radiogenic enrichment, exhumation, and rugged topography. Isotherms are compressed beneath valleys and expanded beneath peaks, with the strongest thermal anomalies localized in the NPM and Karakoram. Surface heat flow patterns reflect these contrasts, ranging from ~120 mW m^{-2} (moderate scenarios) to nearly 180 mW m^{-2} (high exhumation). Crustal differentiation indices further indicate strong upper-crustal enrichment in the NPM and Karakoram, indicating the redistribution of heat-producing elements during crustal thickening and partial melting. The models demonstrate that the region can sustain anomalously high heat flow through the interplay of RHP, exhumation, and crustal differentiation. For northern Pakistan, this provides a robust geoscientific basis for understanding the origin of widespread hydrothermal activity and underscores the region's significant geothermal potential, positioning it as a promising target for future exploration and sustainable energy development.

1 Introduction

Shallow crustal regions of elevated heat flow are typically associated with active volcanism along plate boundaries, representing conventional geothermal resources (Capuno et al., 2010). Recently, ancient cratonic basements have gained attention as potential unconventional geothermal targets (Moeck, 2014). Crystalline rocks such as gneisses and granites often contain high concentrations of radiogenic elements, enhancing heat production and surface heat flow, which makes them promising candidates for hot-dry rock (HDR) geothermal systems (Hillis et al., 2004). Temperatures in HDR systems can reach ~240°C at 3.5 km depth in high heat-producing granitic basements (3.8–8.7 µW m^{-3}), as observed in the Cooper Basin, Australia (Hillis et al., 2004; Beardsmore, 2005; Horspool et al., 2012). Crystalline basements and granitic intrusions, commonly forming the cores of orogenic belts, are large, accessible, and associated with regional orogenic heat flow, making them viable for geothermal exploration (McCay and Younger, 2017; Gnojek et al., 2018; Wanner et al., 2019).

Northern Pakistan lies within the Indian-Asian collision zone, encompassing the Himalaya, Karakoram, and Tibet. More than 500 hot springs occur here, forming the Himalayan Geothermal Belt (Tong & Zang, 1981). This ~3000 km long EW-trending belt extends from the western Himalayas to northwest India and includes parts of the Pamir and Tibet (Fig. 1a). Despite numerous Cenozoic intrusions, the absence of active volcanism and low ^{3}He concentrations suggest a primarily crustal origin of anomalous heat (Hochstein and Zhongke, 1995). Geothermal activity is concentrated along regional faults and suture zones, with hot springs discharging in deeply incised valleys (Hochstein and Regenauer-Lieb, 1998). Interaction of meteoric water with rapidly exhuming hot rocks during ongoing collision explains the hydrothermal activity (Chamberlain et al., 2002).

Comprehensive surface heat flow data are scarce in the Himalaya-Karakoram, limiting knowledge of subsurface geothermal gradients and the lithosphere's thermal state. Available subsurface data—including boreholes, seismic, gravity, and magnetic surveys—are limited, hindering imaging of lithospheric and crustal architecture. While high heat flow (>100 mW m^{-2}) has been reported from geothermal sites in Indian Kashmir (Fig. 1b; Shanker, 1988; Craig et al., 2013), these values may not represent background heat flow due to advective transport in hydrothermal systems. Accurate lithospheric structure and rock properties are essential for thermal modeling, and without them, models only yield broad estimates (Goes et al., 2020).

This study estimates the lithospheric thermal state of the Himalaya, Kohistan, and Karakoram using 1D and 2D thermal models. The models incorporate surface radiogenic heat production, literature-based geophysical parameters, and thermal properties. We assess the influence of variable crustal radiogenic heat production, crustal thickness, and exhumation on geotherms and surface heat flow. Using the 1D models and petrophysical parameters from Anees et al. (2024), 2D models along a cross-section illustrates upper-crustal isotherms and their geothermal implications.

https://doi.org/10.5194/egusphere-2025-5252
Preprint. Discussion started: 17 November 2025

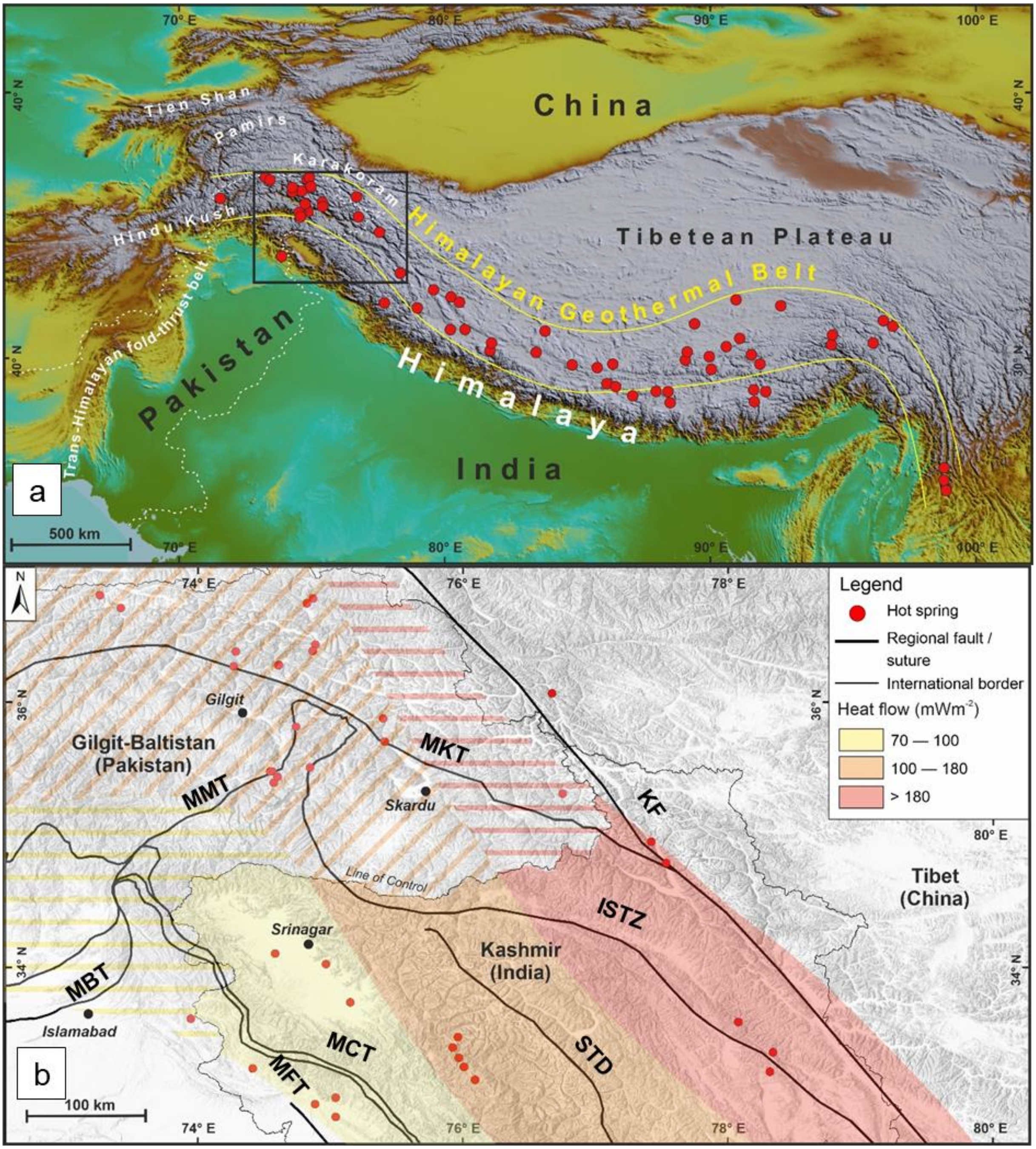

Figure 1: (a) Topographic map of south Asia showing the distribution of hot springs of the Himalaya Geothermal Belt-HGB (after Hochstein & Zhongke, 1995) within the hinterland of India-Asia collision zone. The black rectangle shows the location of Fig 1.1b. (b) Distribution of geothermal manifestations (as hot springs) in the hinterland of western Himalaya and Karakoram and associated interpolated heat flow map (modified after Shanker, 1988; Thussu, 2002; Craig et al., 2013). Heat flow is calculated from geothermal fields in Indian Kashmir and has been projected towards northwest Pakistan (line filled pattern) by Craig et al., 2013. Abbreviations: KF-Karakoram Fault; ISTZ-Indus Tsangpo Suture Zone; MBT-Main Boundary Thrust; MCT-Main Central Thrust; MFT-Main Frontal Thrust; MKT-Main Karakoram Thrust; MMT-Main Mantle Thrust; STD-South Tibet Detachment.

2 Tectonic and Lithospheric Framework

The western Himalayan-Karakoram orogen, forming most of northern Pakistan, is tectonically subdivided from north to south into the Karakoram block (Asian plate), Kohistan (-Ladakh) arc, and the Indian plate (Nanga Parbat Massif) (Gaetani et al., 1996) (Fig. 2a). The Kohistan arc, largely intra-oceanic in origin, was sandwiched between the Asian and Indian plates during the closure of the Neotethys along two suture zones, followed by their collision in the Cenozoic era (Tahirkheli, 1979). These tectonic boundaries are the Main Karakoram Thrust (MKT), separating the Karakoram and Kohistan, and the Main Mantle Thrust (MMT), marking the suture between the Kohistan arc and the Himalayas (Gansser, 1980; Kazmi et al., 1984).

The study area encompasses three tectonic domains: the Nanga Parbat Massif (NPM) of the Himalaya, the Kohistan (-Ladakh) batholith, and the Karakoram batholith. The NPM, the northernmost part of the Himalayas in Pakistan, exposes Proterozoic Indian basement ~~crust~~ up to ~8 km elevation. It has experienced exceptionally high uplift of up to 30 km during the Himalayan orogeny (15 km in the last 3 Ma), forming an N-S striking syntaxis thrusting onto the Kohistan arc (Butler et al., 1989; Zeitler et al., 1993).

The Kohistan-Ladakh arc extends ~700 km in an E-W direction and is positioned between the Karakoram (north, Asian plate) along the Shyok suture zone and the Himalaya (south, Indian plate) along the MMT. This Cretaceous intra-oceanic island-arc complex has been deformed and partly metamorphosed due to obduction onto the Indian plate. Exhumation of the NPM eroded overlying Kohistan crust, splitting it into the Kohistan arc in the west and the Ladakh arc in the east (Tahirkheli, 1979; Petterson, 2010). The Kohistan arc preserves a complete crustal section, from mantle to uppermost crustal rocks, whereas the Ladakh arc predominantly exposes upper crustal volcanic and plutonic rocks (Treloar et al., 1990).

The Karakoram terrane represents the southern margin of the Asian plate and is subdivided into the Northern Karakoram sedimentary belt, Karakoram Batholith, and Karakoram Metamorphic Complex (Searle and Khan, 1996). The northern Karakoram forms a back-arc sedimentary basin with Paleozoic carbonates and clastic deposits extending northward toward the southern Pamir (Palin et al., 2012). The Karakoram Batholith, an E-W trending, 600 km long, and up to 30 km wide axial intrusion, separates the northern sedimentary sequence from the southern metamorphic complex (Searle et al., 1989; Crawford and Searle, 1992). Lithologies include mid-Cretaceous subduction-related granodiorites and diorites in the west and central parts (Hunza plutonic unit) and Jurassic diorite gneisses intruded by post-collisional leucogranites and Miocene syenites in the east (Baltoro plutonic unit, Kande plutonic complex) (Villa et al., 1996; Searle et al., 2010).

The present lithospheric structure reflects these complex subduction and suturing processes (Fig. 2b). Crustal thickening during Himalayan orogeny occurred via underthrusting of the Indian Plate beneath Kohistan and Karakoram. Moho depth increases from 30–40 km beneath the Indian Shield (Acton et al., 2010) to 50–60 km beneath the Himalayan front and 70–80 km within the wedge (Rai et al., 2006; Hazarika et al., 2014; Priestley et al., 2019), with the Indian Plate subducting to >90 km beneath Kohistan and Ladakh (Kufner et al., 2016). Lithosphere-asthenosphere boundary estimates remain variable, between 150–250 km (Li and Mashele, 2009; Kumar et al., 2022; Jadoon et al., 2021), and major suture zones appear decoupled from the lithospheric mantle (Kind and Yuan, 2010; Zhao et al., 2010).

Seismic studies divide the Himalayan crystalline crust into four layers based on P-wave velocities (Guerra et al., 1983; Bhukta et al., 2006). The base consists of upper to mid-crustal metamorphic rocks corresponding to mid-Archean to Neo-Proterozoic shields, overlain by a granulitic lower crust (Grujic et al., 2011; Warren et al., 2011). The Kohistan crust is northward-tilted, exposing upper crustal granitoids and volcanic rocks to the north and mid- to lower-crustal amphibolites and granulites to the south. Its present thickness is ~10–25 km (Malinconico, 1986; Burg et al., 2006; Burg and Bouihol, 2019). Subduction of the Indian lower crust extends as far north as Tibet and the Pamir (Wittlinger et al., 2009; Kumar et al., 2022; Zhao et al., 2010), although the geometry beneath Karakoram and western Tibet remains unresolved. The Karakoram crust comprises a lower crust of unradiogenic felsic and mafic granulites and a radiogenically fertile gneissic middle crust (Searle and Hacker, 2019), with cold, dry granulitic Indian crust likely underlying western Tibet (Priestley et al., 2008). The upper and mid-Indian crust levels beneath Karakoram are believed to have been largely accreted into the Himalayas via lateral material transfer (Razi et al., 2014).

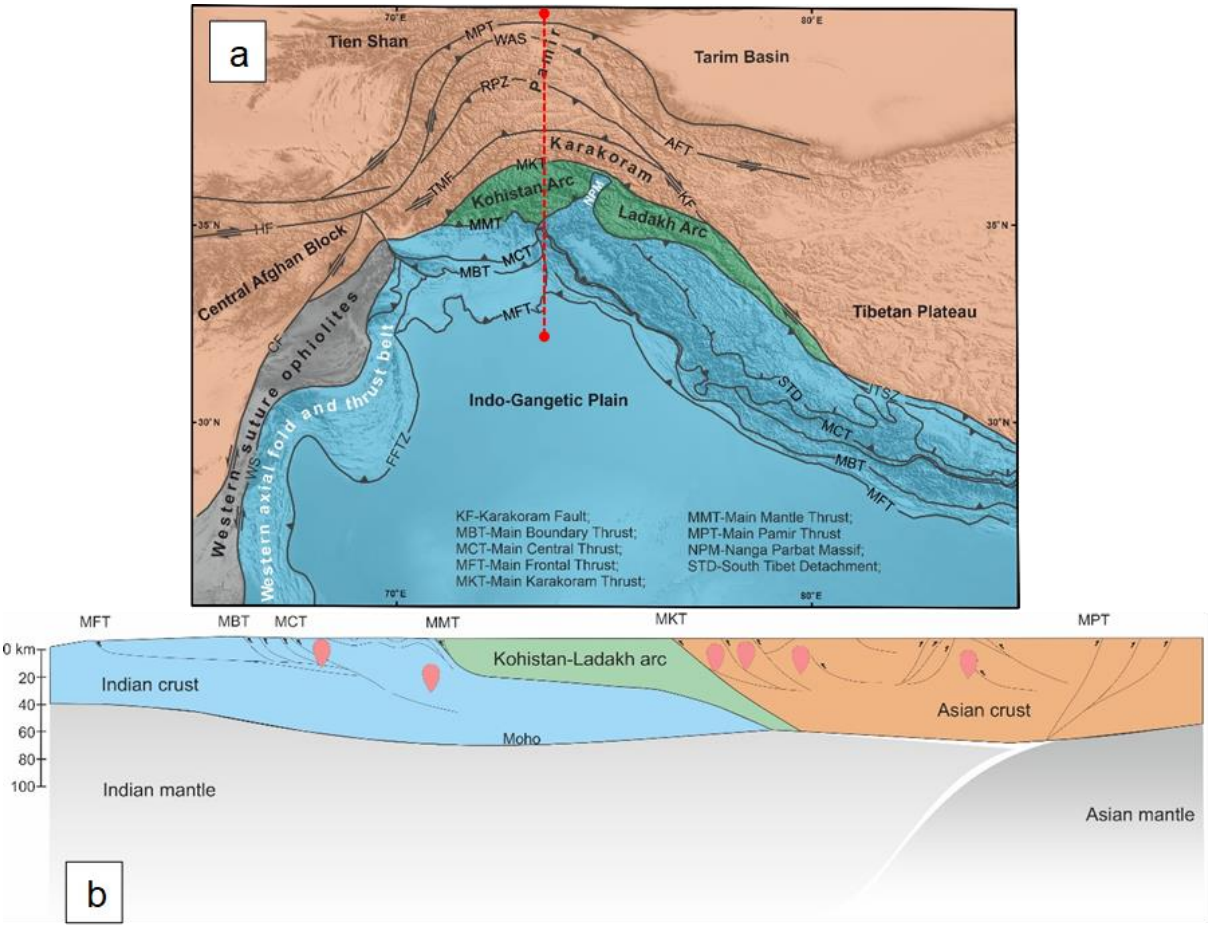

Figure 2: (a) Regional tectonic map of Himalaya and surrounding regions (modified after Beck et al. (1996); Badshah et al. (2000); Dipietro and Pogue (2004); Faisal et al. (2018)). The Kohistan and Ladakh arcs (in green) are sandwiched between the colliding Indian (in blue) and Asian (in orange) plates. The study area comprises the Karakoram, Kohistan-Ladakh arc, and Nanga Parbat Massif. (b) Regional lithospheric structure of Himalaya, Karakoram, and Pamir orogenic belt (after Mechie et al., 2012).

3 1D Steady-State Conductive Thermal Model

This chapter describes the physical and mathematical background of heat transport in solid material as well as the scenarios developed in this work. After introducing the main characteristics of the governing equations for pure heat conduction in 1D, the corresponding scenarios are introduced.

3.1 Mathematical Formulation

A non-linear, steady-state, one-dimensional conductive heat transfer equation is solved as:

$$(k(u)u')' = q, \qquad [1]$$

where u is temperature [K], $k(u)$ is a temperature-dependent thermal conductivity [W m^{-1} K^{-1}], and q is radiogenic heat production [μW m^{-3}], both expressed as functions of depth.

Temperature-dependent thermal conductivity is modeled following Jaupart et al. (2016), with an additional temperature-dependent radiative component at temperatures >1000 K (Jaupart & Mareschal, 2005). The governing equations are:

$$k_u = 2.26 - \frac{618.251}{u} + k_o \cdot \left(\frac{355.576}{u} - 0.30247\right), \text{ and} \qquad [2]$$

$$k_r = 0.37e^{-9} \cdot u^3, u \geq 1000°K, \qquad [3]$$

where k_o is the thermal conductivity of the rock under surface conditions, and k_r represents the radiative contribution at high temperatures. Therefore, the total thermal conductivity is:

$$k(u) = k_u + k_r \qquad [4]$$

Equation (1) is solved using Dirichlet boundary conditions with fixed temperatures at the surface and the base of the lithosphere. The model allows an arbitrary number of layers, each with distinct k_o and q. To handle abrupt changes in properties, a finite-difference “half-station” scheme is employed (Hindle and Besson, 2023). A tri-diagonal matrix algorithm combined with fixed-point iteration solves the non-linear system.

3.2 Modelling Scenarios and Results

Several scenarios were tested to explore the sensitivity of crustal temperatures to key parameters such as lithospheric thickness and upper crustal radiogenic heat production.

3.2.1 Effect of Lithosphere-Asthenosphere Boundary (LAB) depth

Previous studies have used Moho heat flow as a lower boundary for modeling crustal geotherms in parts of the Indian craton (Kumar et al., 2007, 2009). Due to the thicker lithosphere and dynamic orogenic setting in the study area, the LAB at 1300°C is used as the bottom boundary. While the Moho depth is estimated at 60–70 km (Priestley et al., 2019), LAB estimates vary between 150 and 250 km (Li and Mashele, 2009; Jadoon et al., 2021; Kumar et al., 2022).

The effect of this 100 km variation on geotherms was tested with three LAB depths: 150, 200, and 250 km (Fig. 3a). Shallower LAB (150 km) slightly increases temperatures at depth, but its effect on upper crustal temperatures and surface heat flow is negligible. An intermediate LAB depth of 200 km is therefore used in subsequent models.

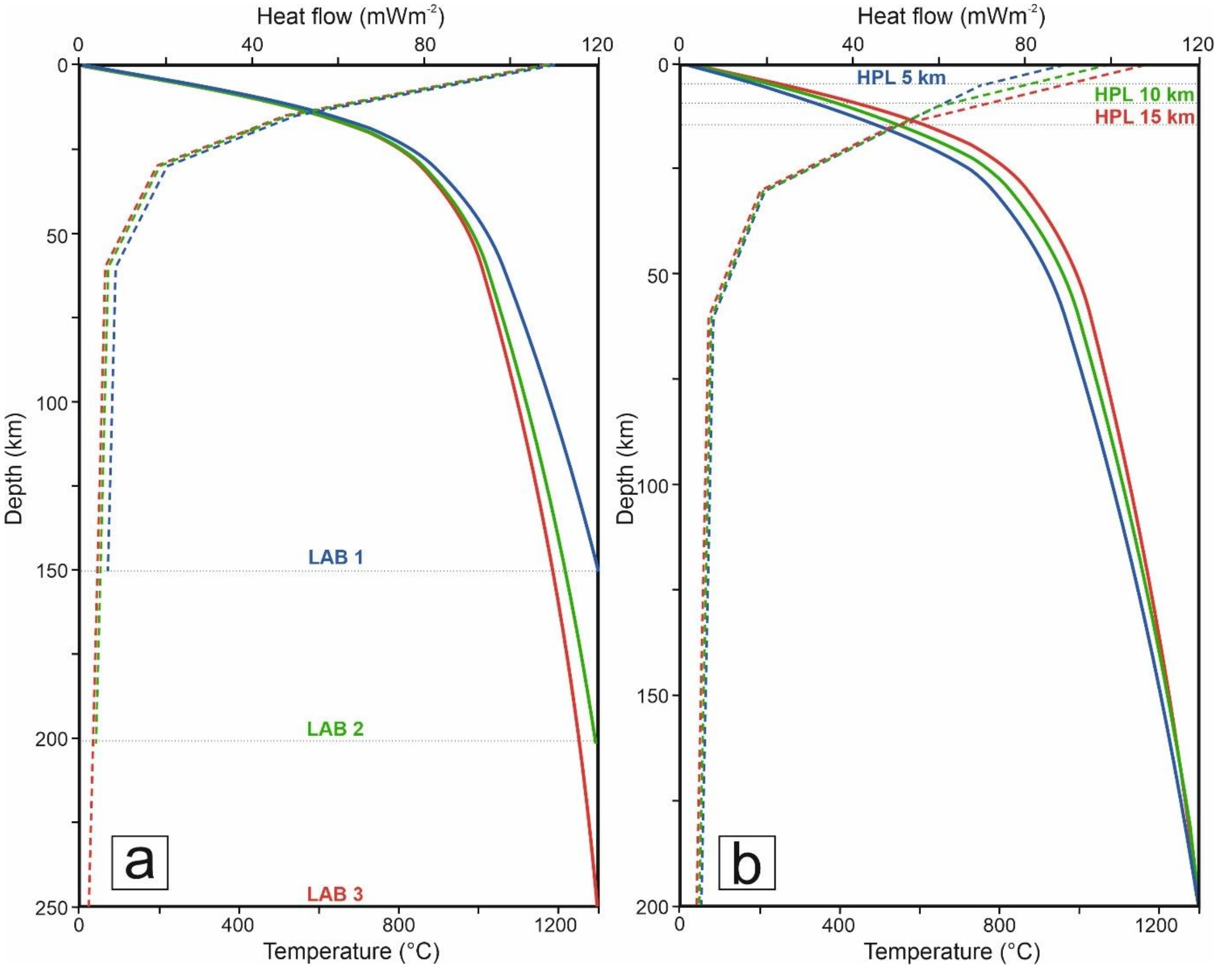

Figure 3: 1D steady-state conductive geotherms showing the effect of thickness of lithospheric and heat-producing layer in the upper crust (a) Geotherms show variations in temperature (as solid lines) and heat flow (as dashed lines) with varying lithospheric thickness from 150 to 250 km. (b) Geotherms show variations in temperature and heat flow with varying thicknesses of heat producing layer in the upper crust from 5 to 15 km.

3.2.2 Effect of Heat-Producing Layer (HPL) Thickness

Radiogenic heat production generally decreases with depth (Jaupart et al., 2016), but vertical and lateral heterogeneity in the upper crust complicates precise stratigraphic control (Vilà et al., 2010). For surface radiogenic heat production, scenarios with variable HPL thicknesses of 5, 10, and 15 km were tested using a mean heat production of 4 $\mu W\ m^{-3}$ (weighted average of the NPM). The crust is modeled as a 25 km thick upper crust (including HPL) overlying a 45 km thick lower crust, with standard heat production values of 0.02, 0.4, and 2 $\mu W\ m^{-3}$ for mantle, lower crust, and upper crust, respectively (Hasterok and

Chapman, 2011). Boundary temperatures are 10°C at the surface and 1300°C at the LAB (McKenzie et al., 2005). Temperature-dependent thermal conductivity and radiative transfer are included.

Results (Fig. 3b) show that a 10 km variation in HPL thickness strongly affects upper crustal geotherms, whereas a 100 km variation in LAB has minimal effect. Calculated temperatures at 10 km depth range from 337°C (HPL = 5 km) to 430°C (HPL = 15 km), increasing to 578–686°C at 20 km depth. Corresponding surface heat flows are 84, 94, and 103 mW m^{-2} for 5, 10, and 15 km thick HPLs, respectively. This highlights the significant role of a thickened heat-producing upper crust in controlling crustal temperatures and surface heat flow.

3.2.3 Nanga Parbat Massif (NPM)

For the 60 km thick crust of the NPM, the lower 30 km is assumed to consist of granulitic rocks with radiogenic heat production of 0.4 μW m^{-3} and thermal conductivity of $Wm^{-1}K^{-1}$ (Roy & Mareschal, 2011). To explore the effect of radiogenic heat distribution in the upper and middle crust, seven models with varying parameters were tested (Fig. S1; Table S1).

Models 1–4 examine the effect of decreasing the thickness of the heat-producing upper crust (4 μWm^{-3}) while increasing the thickness of the mid-crust (with 2 μW m^{-3}). Models 5 and 6 consider a highly enriched upper crust (5.33 μW m^{-3}) with thicknesses of 5 km and 10 km, respectively. Model 7 assumes a 10 km thick enriched upper crust (5.33 μW m^{-3}) combined with a 20 km thick slightly depleted mid-crust. Model 3, representing median parameters, is selected as the preferred scenario (Table 1).

The 1D crustal temperature and surface heat flow profiles for the preferred model are shown in Fig. 4b and 4e (solid blue line), with variations from the other six models shaded. Temperatures at 10 km depth range between 343–506°C across all models, with 405°C for the preferred model. Surface heat flow varies between 85–120 mW m^{-2}, with 100 mW m^{-2} for the median scenario.

3.2.4 Kohistan Arc

The Moho beneath the northern Kohistan arc is estimated at ~70 km depth (Priestley et al., 2019). While the stratigraphic thickness of the arc is 50–55 km (Jagoutz and Schmidt, 2012; Petterson, 2019), the present-day structural thickness is estimated between 10–25 km (Malinconico, 1986; Petterson, 2019). For modeling purposes, the upper crust is assumed to be 20 km thick (Fig. 4a).

Seven scenarios were tested with variable crustal layer thicknesses and radiogenic heat production (Fig. S2; Table S2). In Models 1–5, the upper crust includes felsic (Kohistan batholith) and mafic (amphibolite–granulite) layers, each 10 km thick, with weighted average heat production of 1 μW m^{-3} for felsic rocks and 0.08 μWm^{-3} for mafic rocks (Mukai et al., 1999). The Indian crust, exposed at the NPM in the south, is assumed to underthrust the Kohistan arc and occupy mid-to-lower crustal depths (Searle and Hacker, 2019). The lower crust for all models is similar to the NPM: 30 km thick with 0.4 μW m^{-3}. Mid-crustal layers include two basement components of Indian origin with variable radiogenic heat production.

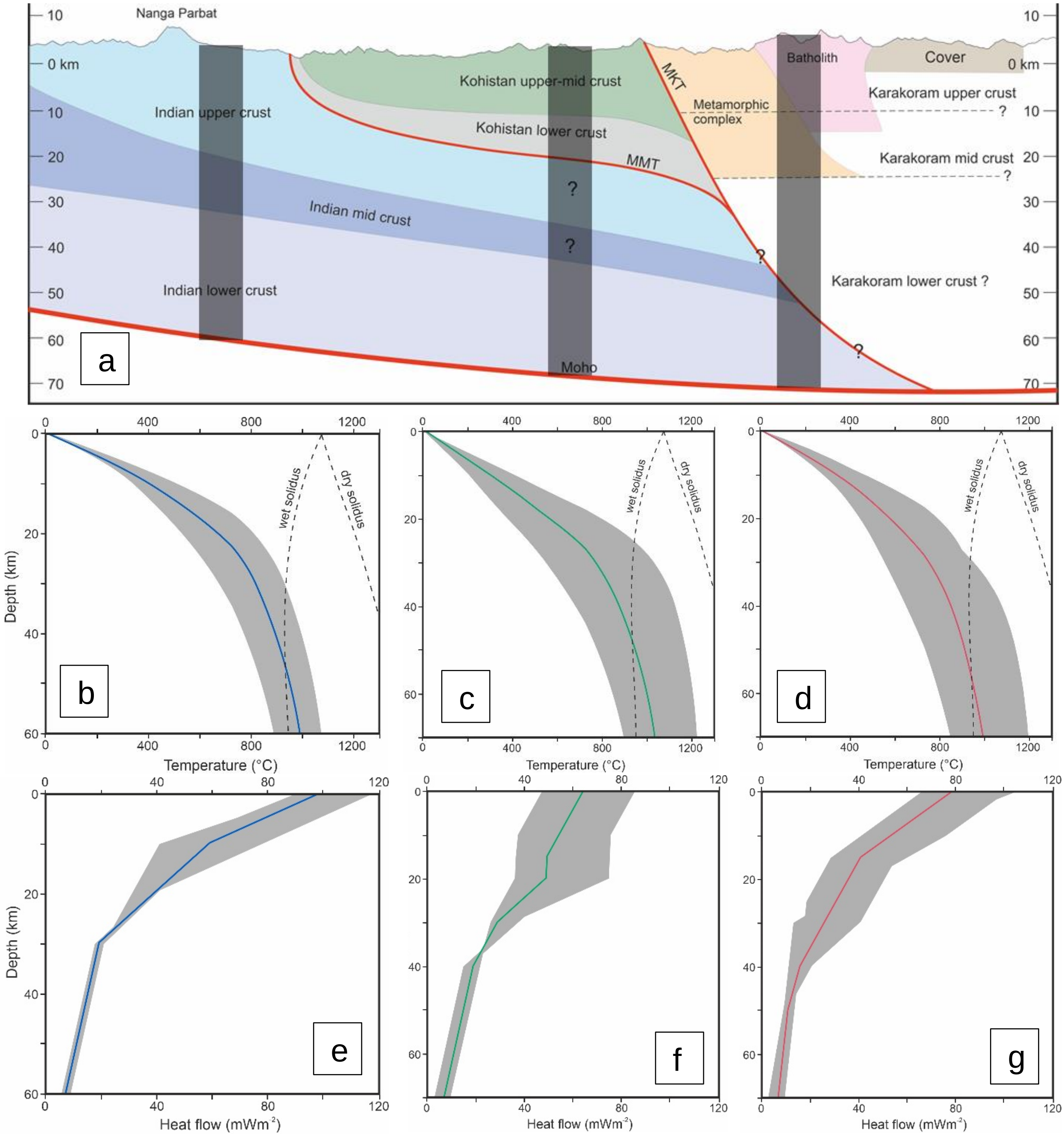

Figure 4: (a) Crustal scale N-S cross-section of the Nanga Parbat Massif, Kohistan, and Southern Karakoram (modified after Searle et al., 2010). The structure of the crust is based on various cross-sections from literature (Searle et al., 1989; Bhukta et al., 2006; Burg et al., 2006; Burg and Bouihol, 2019). Grey columns represent the approximate location of 1D models. 1D steady-state conductive geotherms plots (b, c, d) and surface heat flow (e, f, g) for different modeling scenarios with varying parameters in the Nanga Parbat Massif (b, e), Kohistan arc (c, f) and Karakoram (d, g).

Model 3, with median parameters, is selected as the preferred model for the Kohistan arc (Table 1). The 1D crustal temperature and heat flow profiles for the preferred model are shown in Fig. 4c and 4f (solid green line), with variations from the other six models shaded. Temperatures at 10 km depth vary from 211–413°C across all models, with 299°C for the preferred scenario. Surface heat flow ranges from 50–85 mWm^{-2}, with 65 mWm^{-2} for the median model.

Table 1: Parameters of median steady-state conductive thermal models of the Nanga Parbat Massif, Kohistan arc, and Karakoram based on previous studies (Anees et al., 2023, 2024) and literature (Hasterok and Chapman, 2011; Roy & Mareschal, 2011). Ind-1 and Ind-2, respectively, refer to high and low heat-producing crustal layers. Koh-F and Koh-M, respectively, refer to the upper felsic and lower mafic Kohistan crust overlying the Indian crust. KB-Karakoram batholith, KMC-Karakoram metamorphic complex.

	Thickness (km)	Radiogenic heat production (μW m^{-3})	Thermal Conductivity (W m^{-1} K^{-1})
Nanga Parbat Massif			
Upper crust (Ind-1)	10	4.0	2.3
Mid crust (Ind-2)	20	2.0	2.5
Lower crust	30	0.4	2.6
Kohistan arc			
Upper crust			
Koh-F	10	1.0	2.3
Koh-M	10	0.08	3.0
Mid crust	15	2.0	2.5
Lower crust	30	0.4	2.6
Karakoram			
Upper crust			
KB	15	2.5	2.3
KMC	15	1.0	2.5
Mid crust			
Ind-1	10	1.0	2.3
Ind-2	10	0.5	2.5
Lower crust	20	0.2	2.6

3.2.5 Karakoram

To account for present-day uncertainties in the crustal structure of the Karakoram, seven models were tested with varying parameters (Fig. 4a; Fig S3; Table S3). The total crustal thickness is assumed to be 70 km (Priestley et al., 2019), with a lower depleted crust (0.2 μW m^{-3}) for all models except Model 2. For the upper crust, weighted average radiogenic heat production values of 2.5 μW m^{-3} and 1 μW m^{-3} are assigned to the Karakoram Batholith (KB) and the Karakoram Metamorphic Complex (KMC), respectively. Some models also explored the inclusion of fertile Indian crust at mid-crustal levels, which led to exceptionally high Moho temperatures (~1200°C), requiring readjustment of radiogenic heat production values. Model 3, representing median parameters, is selected as the preferred scenario (Table 1).

The 1D crustal temperature and heat flow profiles for the preferred model are shown in Fig. 4d and 4g (solid green line), with other models depicted as shaded regions. Temperatures at 10 km depth vary between 274–460°C across all scenarios, with 385°C for the median model. Surface heat flow ranges from 65–103 mW m^{-2}, with 80 mW m^{-2} for the median model.

4 1D transient advective-conductive thermal model

We present in this Section the key features of the advection-diffusion heat transfer formulation for the analytical and discretized form and outline the related scenarios.

4.1 Mathematical formulation

A non-linear, transient, one-dimensional heat diffusion equation is solved as:

$$\rho c \frac{\partial u}{\partial t} = (k(u)u')' + q, \qquad [5]$$

where u is temperature [K], $k(u)$ is a temperature-dependent thermal conductivity [W m^{-3} K^{-1}], and q is radiogenic heat production [μW m^{-3}], both functions of depth. ρ is the density [kg m^{-3}] and c is the specific heat capacity [J kg^{-1} K^{-1}].

Equation [5] can be discretized into a recursive, linear system as:

$$\rho c \frac{u_{r+1} - u_r}{\delta t} = (k(u)u')' + q, \qquad [6]$$

where r is the recursive time step. Spatial discretization is performed in fully implicit form:

$$\frac{u_{r+1} - u_r}{\delta t} = A_r u_{r+1} + q_{r+1}, \quad [7]$$

where $A_r = A(u_r)$ is the linearized coefficient matrix dependent on the temperature at the previous time step. Equation [7] can be rearranged as:

$$(I - \delta t A_r)u_{r+1} = u_r + \delta t q_{r+1} \qquad [8]$$

or equivalently $Au = q$. Dirichlet boundary conditions are applied, with fixed temperatures at the top and base of the model. The system is solved recursively using a tri-diagonal matrix algorithm.

4.2 Modelling Scenario

To model the transient effect of exhumation on geotherms in a dynamic orogenic belt, the ideal initial condition would represent the pre-collision state. One approach is to consider the present-day cratonic India as the pre-collision Indian margin and simulate subduction of the Indian passive margin with its cover sediments beneath Kohistan starting at 50 Ma, increasing crustal thickness. However, uncertainties in dynamic and kinematic conditions between 50–10 Ma before the onset of rapid exhumation make this approach challenging (Zeitler et al., 1985). It is also likely that, over ~35 Ma, crustal geotherms re-equilibrated to a near-steady-state condition (Fairley, 2016).

Zircon fission track data (Zeitler et al., 1985) show very young cooling ages (<5 Ma) in the NPM and Karakoram, versus >10 Ma in Kohistan, indicating rapid exhumation (~7 mm y^{-1}) (Fig. 5a). Alternative interpretations suggest slower exhumation between 50–10 Ma followed by constant rates of 3–4 mm y^{-1} over the last 10 Ma (Whittington et al., 1996). Recent petrochronologic and thermal-modeling work documents an ultrafast exhumation pulse in the NPM (~9–13 mm y^{-1} beginning ~1 Ma), preceded by sustained rapid uplift of 2–5 mm y^{-1} (Guevara et al. 2022). However, such high exhumation is localized to the core of the NPM whereas a recent river sediment flux estimate suggesting 3–5 mm y^{-1} as the regional exhumation rate (Clift et al., 2022).

For this work, we do not consider ultrafast exhumation scenario and only test the effect of varying regional exhumation rates and RHP on the temperature and surface heat flow. We use a 1D transient advection-conduction model with parameters listed in Table 2. The upper crust is modeled as a 25 km thick column comprising two layers: 20 km top and 5 km bottom with two RHP scenarios, i.e., 1) High RHP: 4 μW m^{-3} (top), 2 μWm^{-3} (bottom); and 2) Low RHP: 1 μW m^{-3} (top), 0.5 μW m^{-3} (bottom). Boundary conditions are set to 10°C at the top and 800°C at the base to match the metamorphic conditions under the NPM (Crowley et al., 2009; Guevara et al. 2022). Heat advection due to exhumation is implemented via vertical movement (translation) of layers, with the top thinning and the bottom thickening at rates corresponding to the exhumation velocity. The total simulation time is 10 Ma with 1000-year time steps, maintaining a total crustal thickness of 25 km.

Figure 5b and Table 3 summarize the effects of low and high RHP scenarios with exhumation rates of 1–3 mm y^{-1}. Geotherms after 10 Ma are significantly higher than initial conditions. For high RHP models at 3 mm y^{-1}, geotherms invert at 20 km depth. Increasing exhumation rates in low RHP models by 1 mm y^{-1} produces geotherms comparable to high RHP models. At 10 km depth, low RHP geotherms increase by a factor of 1.22, while high RHP models increase by 1.14 per 1 mm y^{-1} increase in exhumation.

Surface heat flow also rises with exhumation. For low RHP models, surface heat flow increases from 75 mW m^{-2} (initial) to 100, 160, and 220 mW m^{-2} for exhumation rates of 1, 2, and 3 mm y^{-1}, respectively. High RHP models show an increase from 110 mW m^{-2} to 135, 180, and 250 mW m^{-2} for the same exhumation rates (Fig. 5c).

Table 2 Parameters used for the 1D transient advective-conductive thermal model to test the effect of exhumation of geotherms and heat flow.

	Crustal depth range (km)	Radiogenic heat production (μWm^{-3})	Thermal Conductivity (Wm^{-1}K^{-1})	Specific heat capacity (J kg^{-1} K^{-1})	Density (kg m^{-3})
Model 1 (High RHP)					
Layer 1	0 – 20	4.0	2.3	750	2700
Layer 2	20 – 25	2.0	2.5	1000	2800
Model 2 (Low RHP)					
Layer 1	0 – 20	1.0	2.3	750	2700
Layer 2	20 – 25	0.5	2.5	1000	2800

Table 3 Results of Temperature (°C) at 10 km for 1D transient advective-conductive thermal model against varying exhumation rates for 10 Ma.

	for exhumation rate				Mean increment factor (per 1 mm y^{-1})
	0 mm y^{-1}	1 mm y^{-1}	2 mm y^{-1}	3 mm y^{-1}	
High RHP model	464	528	611	686	1.14
Low RHP model	348	437	545	630	1.22

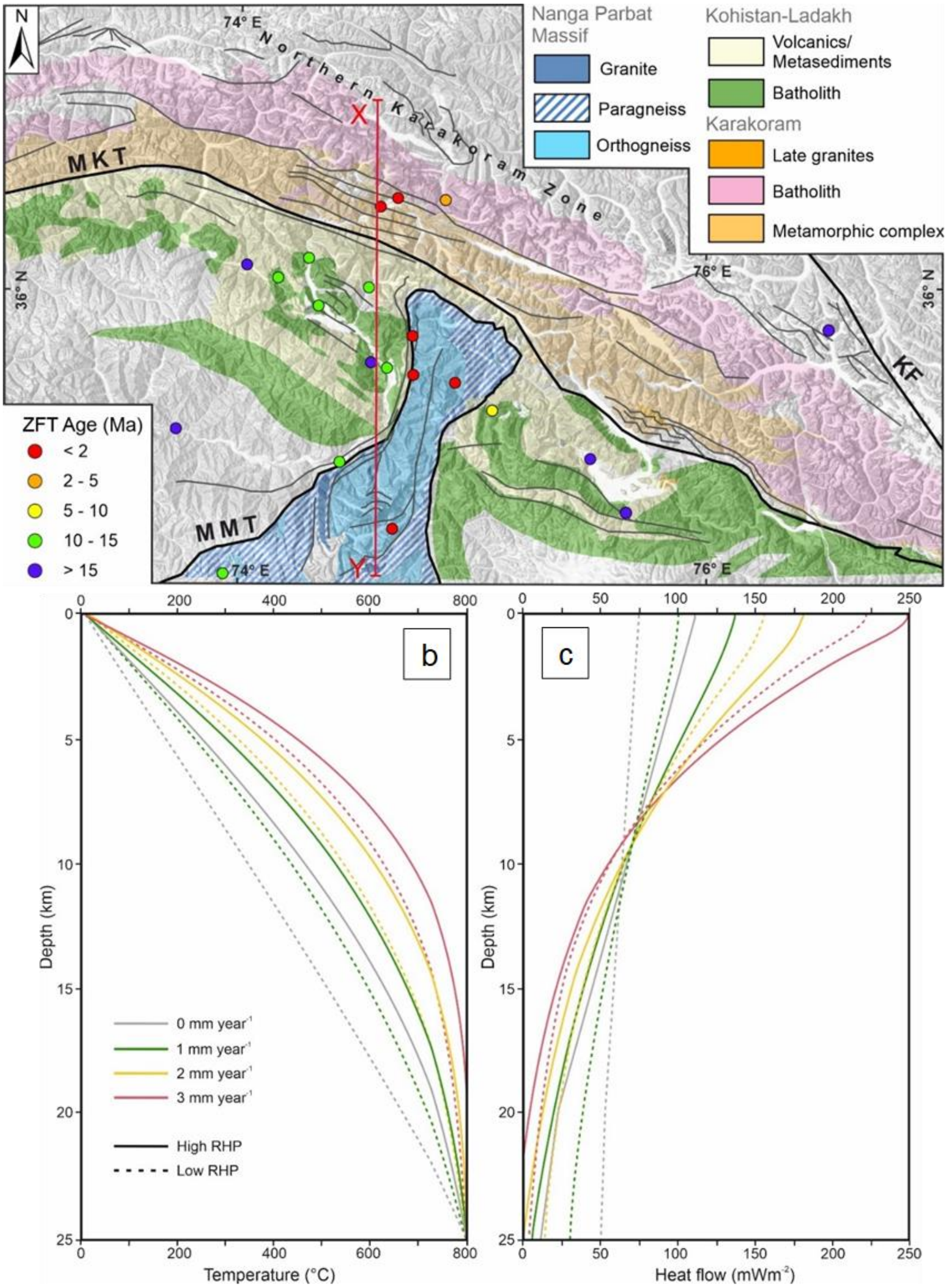

Figure 5: (a) Zircon fission track cooling ages (after Zeitler et al., 1985) in the study area. Young cooling ages show fast exhumation in the Nanga Parbat Massif and Karakoram compared to Kohistan. XY line shows the surface profile of 2D models in Fig 6. (b) 1D transient advective-conductive geotherms and heat flow plots (c) showing the effect of variable exhumation (after 10 Ma) for low (as dashed lines) and high RHP models (as solid lines).

https://doi.org/10.5194/egusphere-2025-5252
Preprint. Discussion started: 17 November 2025

5 2D thermal model

Two-dimensional thermal modeling was conducted to investigate the lateral distribution of isotherms in the upper crust. Exhumation of individual lithospheric blocks has been considered by adding a translational term to the heat conduction equation, resulting in the advection-diffusion equation for the heat transfer. The latter was simulated using a finite element approach implemented in COMSOL Multiphysics®. The model extends to 10 km below sea level along a profile that incorporates representative lithologies and topographic variations (Fig. 6). Petrophysical properties were assigned from outcrop analogs (Anees et al., 2023, 2024) (S2 Table 5). To account for temperature-dependent thermal conductivity, the formulation of Jaupart et al. (2016) was implemented in COMSOL Multiphysics® through an analytical function. The final triangular finite-element mesh consists of 72,643 elements, covering an area of 2,255 km² (Fig. 6).

Boundary conditions include thermally insulated lateral margins and a fixed temperature of 0 °C at the surface. At the basal boundary (10 km bsl), laterally variable temperatures were imposed, derived from the median 1D transient models for the Nanga Parbat Massif (NPM), Kohistan, and Karakoram (S2 Table 4). Three scenarios were evaluated to test the influence of exhumation and radiogenic heat production (RHP).

The modeled geotherms reveal marked contrasts in thermal structure depending on the imposed parameters (Fig. 7). In all cases, isotherms are compressed toward the surface, with shallow isotherms tracking the topography. The effect of relief is particularly evident in the NPM and Karakoram, where isotherms are deflected upward beneath valleys and expand beneath peaks.

Model 1 (high exhumation, low RHP) generates the warmest upper crust beneath the NPM, with 10 km temperatures exceeding 600 °C at an exhumation rate of 3 mm y^{-1}. Here, relatively rapid exhumation drives strong advective heat transfer, outperforming the weak radiogenic contribution. The anomaly is spatially confined to the NPM, consistent with focused exhumation.

Model 2 (low exhumation, high RHP) also produces high upper-crustal temperatures (~520–570 °C at 10 km beneath the NPM), but the elevated geotherms are maintained by radiogenic heating. The anomaly is broader and less localized than in Model 1, reflecting the more diffusive nature of radiogenic heat production.

Model 3 (low exhumation, moderate RHP) represents an intermediate state, with 10 km depth temperatures of ~450–480 °C beneath the NPM. Neither exhumation nor RHP alone generates the extreme anomalies of Models 1 and 2, yielding a more subdued thermal field.

These contrasts are reflected in the modeled surface heat flow distributions (Fig. 7). At the NPM, values range from ~120 mW m^{-2} in Model 3 to nearly 180 mW m^{-2} in Model 1, capturing the strong sensitivity of surface heat flow to exhumation and RHP. By comparison, Kohistan exhibits relatively uniform values (60–90 mW m^{-2}) across scenarios, while the Karakoram displays a modest increase to 100–120 mW m^{-2}. Collectively, the results demonstrate that either rapid exhumation or high RHP can independently produce elevated geotherms beneath the NPM, though their effects differ in spatial expression and magnitude.

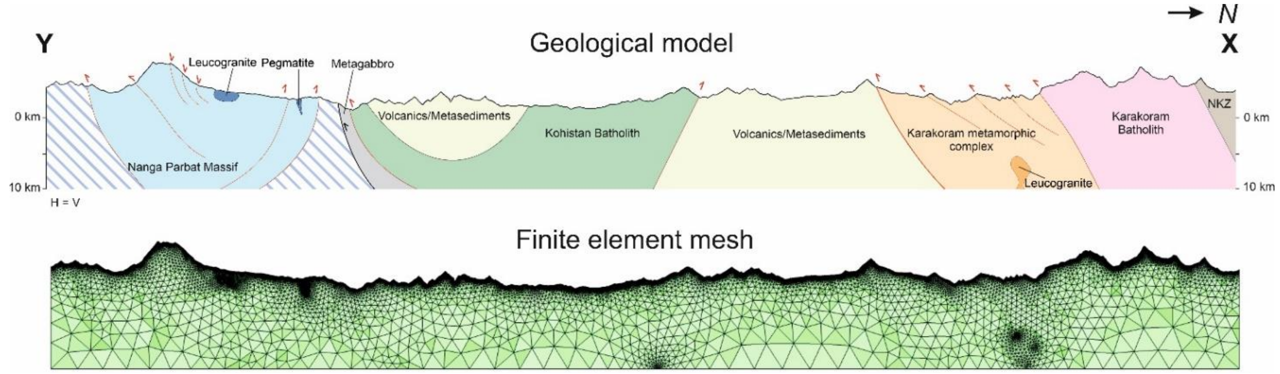

Figure 6: Top: Geological model of the XY profile in Fig 5a showing the subsurface geological structure of the major lithological units up to 10 km below sea level (modified after Searle & Khan, 1996). Bottom: Two-dimensional triangular finite-element mesh containing 72643 elements created in COMSOL Multiphysics® for the dynamic thermal modelling.

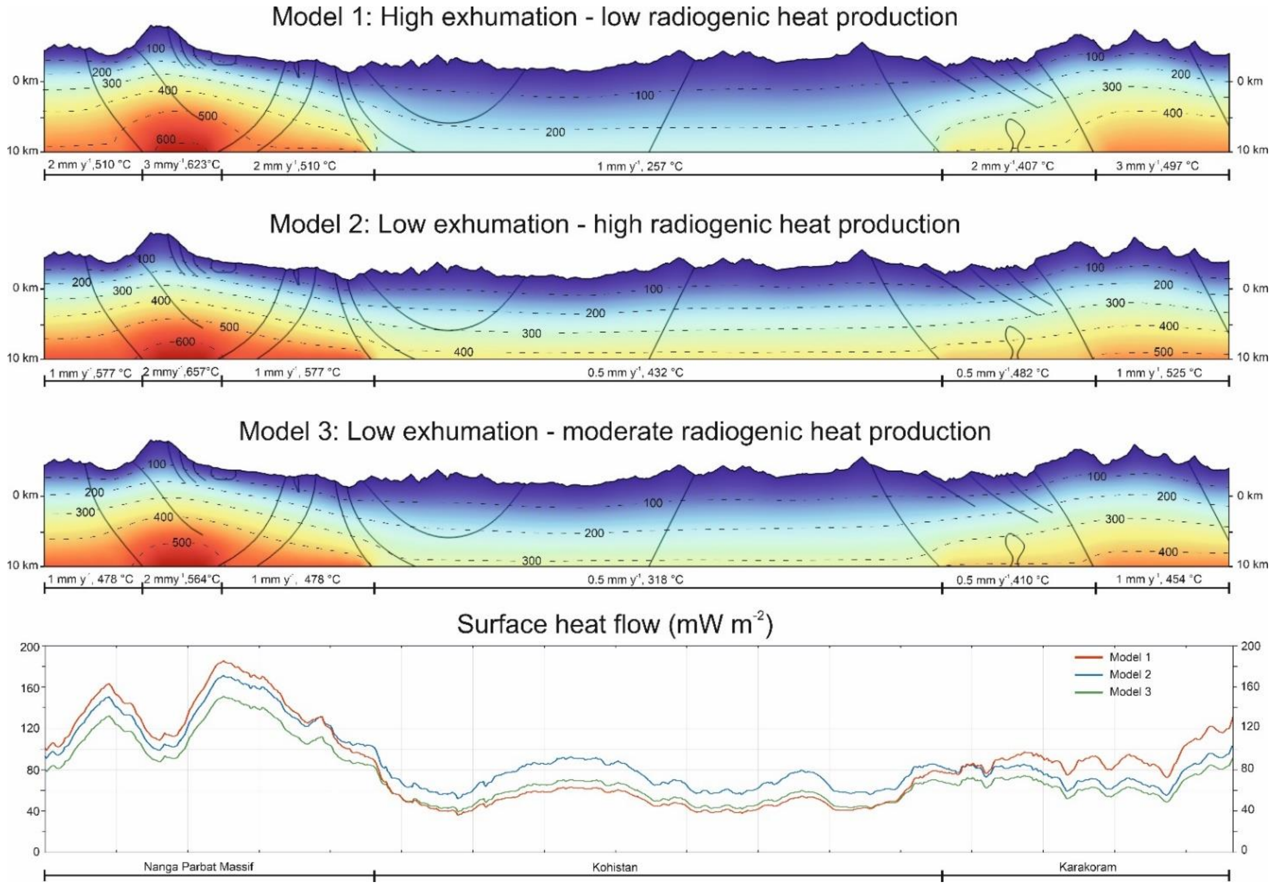

Figure 7: 2D simulation results showing subsurface temperature distribution and surface heat flow with basal temperature input from 1D transient advective-conductive models, which test combination of variable exhumation and radiogenic heat production scenarios for the Nanga Parbat Massif, Kohistan and Karakoram. Advective and diffusive heat transfer is accounted for by modeling the translation of the respective lithospheric blocks during exhumation.

6 Discussion

6.1 Thermal Modeling of the Lithosphere and Radiogenic Heat Production

The tectonic framework of the Himalaya–Kohistan–Karakoram system exerts a profound influence on its present-day thermal state. Subduction and imbrication of the Indian plate have produced substantial crustal thickening, while subsequent exhumation has advected heat toward the surface. These processes act in tandem: thickening enhances the integrated radiogenic heat production (RHP) of the crust (Jaupart et al., 2016), whereas exhumation rapidly transports hot rocks upward, generating strong near-surface anomalies (Jamieson et al., 2002). Additionally, thickened crust fosters partial melting at depth, with melts emplaced as plutons in the upper crust (Jamieson et al., 2011). Collectively, these mechanisms explain why orogenic belts are typically associated with deep Moho, shallow Curie depths (~580 °C isotherm), and anomalously high background heat flow (Gao et al., 2017).

Developing reliable lithospheric thermal models therefore requires robust constraints on crustal structure and physical properties. In stable cratonic settings, this is feasible because steady-state models can be anchored to deep borehole heat-flow data, which minimize transient near-surface effects (Fuchs et al., 2022). In contrast, active orogens such as the Himalaya lack reliable surface heat-flow datasets and suffer from poorly constrained geophysical profiles at depth. The present study addresses this challenge by adopting a suite of models with variable parameters, thereby bracketing the plausible thermal states of the lithosphere rather than committing to a single deterministic solution.

Within thermal models of the continental crust, RHP is widely regarded as the dominant parameter controlling crustal geotherms (Hasterok & Chapman, 2011). However, its vertical distribution remains ambiguous. It is generally accepted that lower crustal melting and melt extraction redistribute heat-producing elements upwards in the crust, leading to depletion in the lower crust and enrichment in the upper layers (McKenzie & Priestley, 2016). However, at mid-crustal level, this redistribution is neither complete nor uniform—particularly during near- or sub-solidus partial melting. In such conditions, thorium can be retained in resilient accessory minerals (e.g., monazite, zircon, allanite), enabling migmatitic rocks to maintain high RHP even when U and K are removed with melt extraction (Alessio et al., 2018; Yakymchuk & Brown, 2019; Weller et al., 2020). This aligns with global datasets, which show no systematic decline in RHP with increasing metamorphic grade (Hasterok et al., 2018). Our previous work corroborates this interpretation, revealing elevated Th concentrations in migmatitic gneisses from the region (Anees et al., 2023).

The present modeling approach provides a critical evaluation of these hypotheses. Assigning surface-derived RHP values uniformly through the crust produces unrealistically hot geotherms (Fig. 4; Fig. S2), with Moho temperatures far exceeding petrological and geophysical constraints. This strongly suggests that RHP diminishes with depth in active orogens, likely through fractionation, melt extraction, and redistribution processes. At the same time, localized upper-crustal enrichment by pluton emplacement may sustain high surface values. Thus, the results argue against simplistic uniform-depth assumptions and instead favor models that incorporate depth-dependent variability in RHP.

6.2 Crustal Differentiation

The distribution of heat-producing elements in the crust provides an important window into its differentiation history. Perry et al. (2006a) proposed a crustal differentiation index (D_I) to indicate vertical stratification in the crust in response to the enrichment of upper crustal layers. They derived D_I through a ratio of mean surface heat production (A_o) and total mean crustal heat production (A_c) as follows;

$$D_I = \frac{A_o}{A_c}$$

$$A_c = \frac{Q_s - Q_m}{h}$$

where, Q_s is the surface heat flow, Q_m is the heat flow from the mantle, and h is the crustal thickness.

In the absence of surface heat flow data, the values calculated from 1D steady-state models are incorporated for the calculation of D_I. For the NPM, the total mean crustal heat production (1.5 μW m^{-3}) is obtained by removing the mean mantle heat flow (8 mW m^{-2}) from the mean surface heat flow (100 mW m^{-2}) and dividing it by total crustal thickness (60 km). The ratio of total mean crustal heat production (1.5 μW m^{-3}) and mean surface heat production (4.6 μW m^{-3}) provides a D_I of 3. Similarly, the D_I for Kohistan and Karakoram are calculated to be 1.1 and 2, respectively.

Figure 7 shows a plot of differentiation index (D_I) vs. bulk mean crustal heat production (A_c) for the NPM, Kohistan, and Karakoram and compares them with the Indian (Bundelkhand and Dharwar) and North American (Trans-Hudson, Grenville, and Appalachians) cratons (Perry et al., 2006a; Podugu et al., 2017). The plot shows a positive correlation between D_I and mean crustal heat production, with $D_I > 1$ suggesting radiogenic radioelement enrichment in the upper crust, possibly due to magmatic differentiation (Perry et al., 2006a). The higher D_I in the NPM (3) and Karakoram batholith (2) is comparable to Appalachians (2.5), indicating enrichment of radioelements in the upper crust. In comparison, the Kohistan batholith shows low D_I (1.1), which is on par with the Dharwar craton, Grenville Province and Trans-Hudson Orogen. However, the Kohistan batholith shows higher average crustal heat production compared to these Indian and North American terranes, which can be attributed to the subducting enriched Indian crust under it.

The D_I values of the NPM and Bundelkhand craton are equally high, but the significantly higher average crustal heat production in the NPM (1.5 μW m^{-3}) compared to Bundelkhand craton (0.41 – 0.68 μW m^{-3}) can be associated with the imbrication and crustal thickening. Doubling the crustal thickness also doubles its average crustal heat production, which results in high temperatures at mid to lower crust depths. This triggers crustal melting, in which radioelements are redistributed by migrating upwards in the upper crust, thus stabilizing the temperatures in the lower crust (Perry et al., 2006a). This is also corroborated by our modeling results, where higher RHP (≥ 2 μW m^{-3}) layers in the mid-crust provided exceptionally hot geotherms (Fig 4; Fig. S2). It should be noted that, in the absence of surface heat flow measurements, the estimations of differentiation index and average crustal heat production should be considered preliminary.

Recent thermomechanical models further emphasize the role of radiogenic enrichment in the upper crust. Fan et al. (2024) demonstrated that sustained ultra-high temperature metamorphism in the Greater Himalayan Crystalline Complex was

https://doi.org/10.5194/egusphere-2025-5252
Preprint. Discussion started: 17 November 2025

primarily driven by elevated radiogenic heat production (~4 μW m⁻³) in a partially molten upper crust, with mechanical heating playing only a transient role during the early stages of collision. This highlights that crustal differentiation, whereby heat-producing elements are preferentially concentrated in the upper crust through partial melting and magmatic segregation, can maintain high geotherms over tens of millions of years. Such findings are consistent with our results, where high D_I in the NPM and the Karakoram reflect strong upper-crustal enrichment in radiogenic elements, enhancing both thermal gradients and geothermal potential

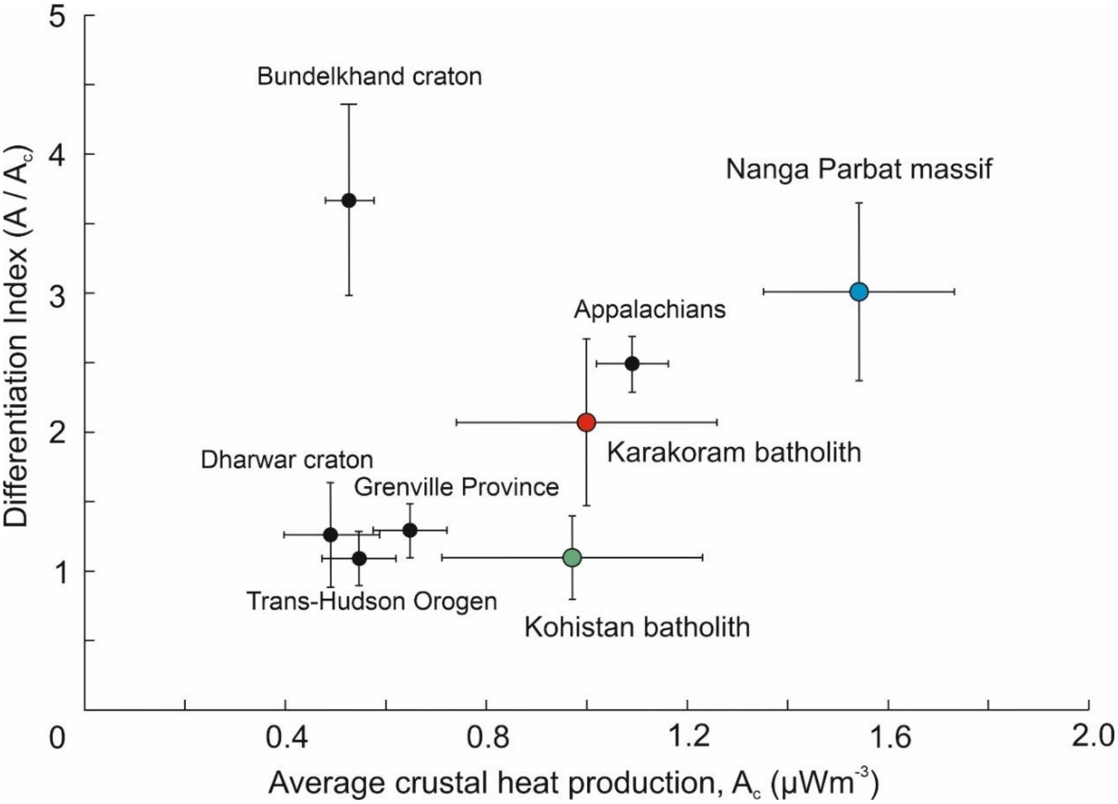

Figure 8: Plot of differentiation index (D_I) vs. average crustal heat production (A_c) for the Nanga Parbat Massif, Kohistan and Karakoram batholith in comparison with Indian shields (after Podugu et al., 2017) and North American geological provinces (after Perry et al., 2006a).

6.3 Upper Crustal Heat Flow and Geothermal Implications

1D modeling results indicate that surface heat flow is strongly controlled by the thickness and intensity of heat-producing layers in the upper crust. While transient 1D models emphasize the influence of exhumation, 2D models reveal that its lateral impact is limited compared to radiogenic heat production (RHP). In the NPM, a high thermal regime results from the combined effects of exhumation and RHP, producing elevated near-surface geothermal gradients. Topographic relief further modulates near-surface temperatures, explaining the spatial distribution of hot springs.

These hot springs typically occur in zones of enhanced permeability, such as faults, efficiently tapping areas of locally increased heat production. In addition, unlike purely conductive heat transport, topography-driven deep groundwater flow interacting with heat-producing rocks promotes advective heat transfer to the surface. This advective process is more efficient and rapid, particularly in evolving orogens (Chamberlain et al., 1995; Wanner et al., 2020).

The regional geothermal regime indicates medium to high enthalpy potential. Rivers such as the Indus and Astore cut across the NPM at elevations of 1150–2500 m a.s.l., placing the 100 °C isotherms near the surface and potentially providing access to > 200 °C within 3 km depth. Even under conservative estimates of exhumation and RHP, isotherms exceeding 100 °C are predicted in the range of 1200–2500 m depths in the valleys. Additionally, subsurface groundwater aquifers in high-relief areas maintain elevated temperatures due to their extended and deeper flow paths.

Consequently, the primary geothermal resources in the region are likely petrothermal (hot-dry rock) and hydrothermal (hot aquifer) systems, reflecting both the elevated crustal heat production and favorable hydrogeologic conditions.

6.4 Modelling Limitations

The thermal models presented here explore the potential role of radiogenic heat production (RHP) and provide first-order estimates of crustal geotherms and surface heat flow, while accounting for uncertainties arising from limited data and heterogeneous parameters. In these models, intra-layer RHP values are assumed constant. However, as noted in Section 7.2, assigning surface RHP values to mid-crustal layers leads to unrealistically high temperatures. Accordingly, mid-crustal RHP values were adjusted to produce reasonable geotherms consistent with stratified continental crust models (Rudnick & Gao, 2003; Hacker et al., 2015).

In active collisional settings, additional dynamic and transient processes can influence crustal heat production and heat flow, including uplift, shear heating, partial melting and melt migration, crustal thickening, and paleoclimate effects. Shear heating is significant in fault zones during orogenic evolution (Burg & Gerya, 2005; Wang et al., 2013; Ai et al., 2021), but its crustal-scale contribution is negligible compared to radiogenic heat (Fagereng & Biggs, 2019). Melt migration from mid-crustal anatexis can advect heat to the upper crust, but in the present case, its effect is spatially limited and neglected. Crustal thickening increases the total radiogenic content but is also excluded due to its long timescale relative to model duration.

Lateral and vertical lithological variations, along with deformation intensity, strongly influence rock properties and can significantly affect local heat flow (Abdulagatova et al., 2020; Weinert et al., 2020). Thermophysical parameters used in the 2D model, derived from outcrop analogs, do not fully represent deep-crustal conditions affected by temperature, pressure, and fluids. Fluid circulation and rock permeability are not included; cold meteoric water percolation can cause hydrothermal cooling and locally reduce conductive geotherms (Cao et al., 2019). Conversely, in hot spring areas, upward advection of heat by fluids can elevate near-surface temperatures and disturb conductive heat flow (Bächler et al., 2003; Koltzer et al., 2019). Consequently, regions with high deformation and fracture-related permeability are most susceptible to advective heat transport.

7 Conclusion

This study investigated the interplay of radiogenic heat production (RHP) and exhumation in shaping the thermal structure of the Nanga Parbat Massif (NPM), Kohistan, and Karakoram, with a particular focus on their geothermal implications. Given the limited direct heat flow measurements and the uncertainty in lithospheric structure, we applied multiple steady-state, transient, and two-dimensional thermal models to evaluate a range of plausible scenarios.

The results emphasize that surface RHP values cannot be directly extrapolated to the mid- and lower crust, particularly in tectonically active, subducting, or underthrust settings where redistribution of heat-producing elements occurs via partial melting and differentiation. Instead, surface heat flow is strongly governed by the thickness and enrichment of upper-crustal heat-producing layers. Exhumation enhances heat advection by transporting hot material upward, thereby amplifying surface heat flow even where upper-crustal RHP is modest. However, its thermal influence is spatially localized, primarily confined to regions directly above rapidly uplifting blocks such as the NPM. By contrast, RHP exerts a broader and more sustained lateral influence on geotherms across the entire crust.

Simulations results based on two-dimensional advection-diffusion models further reveal the strong imprint of topography on near-surface thermal fields. Isotherms expand beneath topographic highs and are compressed beneath valleys, producing localized zones where elevated geothermal gradients occur at shallower depths. Such structural–topographic interactions suggest that deep valleys, particularly in the NPM and Karakoram, represent optimal sites for accessing high-temperature reservoirs through relatively shallow drilling.

Taken together, these findings demonstrate that the collisional setting of northern Pakistan sustains anomalously high heat flow not through magmatism, but through the combined effects of radiogenic enrichment, crustal thickening, and rapid exhumation. The thermal regime revealed by our models provides a geodynamic explanation for the widespread occurrence of hot springs in the region and underscores the underexplored geothermal potential of collisional orogens. Importantly, valleys within the NPM and Karakoram emerge as prime targets for geothermal exploration, offering opportunities for sustainable energy development in a tectonic setting traditionally overlooked in geothermal assessments.

Code availability

The code used for 1D thermal modelling is available online on Zenodo (https://doi.org/10.5281/zenodo.7875951) and on Github (https://github.com/davidhindle/steady-nl-heat/tree/steady-nl-heat).

Author contribution

Muhammad Anees: Conceptualization, Methodology, Investigation, Formal analysis, Visualization, Validation, Writing (original draft preparation), Writing (review and editing), Funding acquisition, Project administration. **David Hindle:** Conceptualization, Data curation, Methodology, Validation, Writing (review and editing), Resources, Software. **Ernesto**

Meneses Rioseco: Methodology, Validation, Writing (review and editing), Resources, Software. **Jonas Kley:** Writing (review and editing), Supervision, Project administration, Funding acquisition. **Bernd Leiss:** Writing (review and editing), Supervision, Project administration, Conceptualization. **Mumtaz M. Shah:** Writing (review and editing), Supervision. **Javed Akhter Qureshi:** Writing (review and editing), Resources.

Competing interests

The authors declare that they have no conflict of interest.

Acknowledgements

This study was funded through a doctoral fellowship (91725964) by the DAAD (Deutscher Akademischer Austauschdienst), supported by the German Federal Ministry of Education. Additional financial support was provided by the DFG (Deutsche Forschungsgemeinschaft; Project KL 495/32–1).

The authors also acknowledge the use of artificial intelligence tools (e.g., ChatGPT by OpenAI) to improve the clarity and language of the manuscript. The scientific interpretations, results, and conclusions remain entirely the authors' own.

References

Acton, C. E., Priestley, K., Gaur, V. K., and Rai, S. S.: Group velocity tomography of the Indo-Eurasian collision zone, J. Geophys. Res. Solid Earth, 115, B12, 2009JB007021, https://doi.org/10.1029/2009JB007021, 2010.
Ai, Y., Zhang, J., Dong, M., Wang, B., and Fang, G.: Heat generation effects from shear friction along Xianshui river strike-slip fault in western Sichuan, China, Geothermics, 89, 101936, 2021.
Alessio, K. L., Hand, M., Kelsey, D. E., Williams, M. A., Morrissey, L. J., and Barovich, K.: Conservation of deep crustal heat production, Geology, 46, 335–338, 2018.
Anees, M., Kley, J., Leiss, B., Hindle, D., Wajid, A.A., Wagner, B., Shah, M.M. and Luijendijk, E.: Application of in-situ gamma spectrometry for radiogenic heat production estimation in the Western Himalaya, Kohistan, and Karakoram in northern Pakistan. Geothermal Energy, 11(1), 2023.
Anees, M., Sosa, G., van den Kerkhof, A., Leiss, B., Kley, J., Shah, M. M., and Weydt, L. M.: Granitoids of the western Himalaya and Karakoram as potential geothermal reservoirs – A petrological, geochemical and petrophysical study, Geothermics, 121, 103040, 2024.
Artemieva, I. M., Thybo, H., Jakobsen, K., Sørensen, N. K., and Nielsen, L. S.: Heat production in granitic rocks: Global analysis based on a new data compilation GRANITE2017, Earth-Sci. Rev., 172, 1–26, 2017.
Bächler, D., Kohl, T., and Rybach, L.: Impact of graben-parallel faults on hydrothermal convection—Rhine Graben case study, Phys. Chem. Earth, 28, 431–441, 2003.
Beardsmore, G. R.: Thermal modelling of the hot dry rock geothermal resource beneath GEL99 in the Cooper Basin, Proc. World Geotherm. Congr., Antalya, Turkey, 24–29 April, 2005.
Bhukta, S. K., Sain, K., and Tewari, H. C.: Crustal Structure Along the Lawrencepur-Astor Profile in the Northwest Himalayas, Pure Appl. Geophys., 163, 1257–1277, https://doi.org/10.1007/s00024-006-0070-x, 2006.
Burg, J., Jagoutz, O., Dawood, H., and Hussain, S. S.: Precollision tilt of crustal blocks in rifted island arcs: Structural evidence from the Kohistan Arc, Tectonics, 25, 2005TC001835, https://doi.org/10.1029/2005TC001835, 2006.
Burg, J.-P., and Gerya, T. V.: The role of viscous heating in Barrovian metamorphism of collisional orogens:

Thermomechanical models and application to the Lepontine Dome in the Central Alps, J. Metamorph. Geol., 23, 75–95, https://doi.org/10.1111/j.1525-1314.2005.00563.x, 2005.

Burg, J.-P., and Bouilhol, P.: Timeline of the South Tibet–Himalayan belt: The geochronological record of subduction, collision, and underthrusting from zircon and monazite U–Pb ages, Can. J. Earth Sci., 56, 1318–1332, 2019.

Burtman, V. S., and Molnar, P.: Geological and geophysical evidence for deep subduction of continental crust beneath the Pamir, 1993.

Butler, R. W.: Tectonic evolution of the Himalayan syntaxes: The view from Nanga Parbat, Geol. Soc., Lond., Spec. Publ., 483, 215–254, 2019.

Butler, R. W., and Prior, D. J.: Tectonic controls on the uplift of the Nanga Parbat Massif, Pakistan Himalayas, Nature, 333, 247–250, 1988.

Butler, R. W., Prior, D. J., and Knipe, R. J.: Neotectonics of the Nanga Parbat syntaxis, Pakistan, and crustal stacking in the Northwest Himalayas, Earth Planet. Sci. Lett., 94, 329–343, 1989.

Cao, W., Lee, C.-T. A., Yang, J., and Zuza, A. V.: Hydrothermal circulation cools continental crust under exhumation, Earth Planet. Sci. Lett., 515, 248–259, 2019.

Chamberlain, C. P., Zeitler, P. K., Barnett, D. E., Winslow, D., Poulson, S. R., Leahy, T., and Hammer, J. E.: Active hydrothermal systems during the recent uplift of Nanga Parbat, Pakistan Himalaya, J. Geophys. Res. Solid Earth, 100, 439–453, 1995.

Clift, P.D., Mark, C., Alizai, A., Khan, H. and Jan, M.Q.: Detrital U–Pb rutile and zircon data show Indus River sediment dominantly eroded from East Karakoram, not Nanga Parbat. Earth and Planetary Science Letters, 600, p.117873, 2022.

Craig, J., Absar, A., Bhat, G., Cadel, G., Hafiz, M., Hakhoo, N., Kashkari, R., Moore, J., Ricchiuto, T. E., and Thurow, J.: Hot springs and the geothermal energy potential of Jammu & Kashmir State, NW Himalaya, India, Earth-Sci. Rev., 126, 156–177, 2013.

Crawford, M. B., and Searle, M. P.: Field relationships and geochemistry of pre-collisional (India-Asia) granitoid magmatism in the central Karakoram, northern Pakistan, Tectonophysics, 206, 171–192, 1992.

Crowley, J.L., Waters, D.J., Searle, M.P. and Bowring, S.A.: Pleistocene melting and rapid exhumation of the Nanga Parbat massif, Pakistan: Age and P–T conditions of accessory mineral growth in migmatite and leucogranite. Earth and Planetary Science Letters, 288(3-4), pp.408-420, 2009.

Debon, F., Le Fort, P., Dautel, D., Sonet, J., and Zimmermann, J. L.: Granites of western Karakorum and northern Kohistan (Pakistan): A composite Mid-Cretaceous to upper Cenozoic magmatism, Lithos, 20, 19–40, 1987.

Fagereng, Å., and Biggs, J.: New perspectives on 'geological strain rates' calculated from both naturally deformed and actively deforming rocks, J. Struct. Geol., 125, 100–110, 2019.

Fairley, J. P.: Models and modeling: An introduction for Earth and environmental scientists, John Wiley & Sons, 2016.

Fan, Y.L., Zhang, L.F., Wang, Y. and Li, Z.H.: Role of crustal radiogenic heating in ultra-high temperature metamorphism of the Greater Himalayan Crystalline complex: Phase equilibrium and numerical modelling. Gondwana Research, 125, pp.301-316, 2024.

Fuchs, S., Förster, A., and Norden, B.: Evaluation of the terrestrial heat flow in Germany: A case study for the reassessment of global continental heat-flow data, Earth-Sci. Rev., 235, 104231, 2022.

Furlong, K. P., and Chapman, D. S.: Heat Flow, Heat Generation, and the Thermal State of the Lithosphere, Annu. Rev. Earth Planet. Sci., 41, 385–410, 2013.

Gaetani, M., Angiolini, L., Nicora, A., Sciunnach, D., Le Fort, P., Tanoli, S., and Khan, A.: Reconnaissance geology in Upper Chitral, Baroghil and Karambar districts (northern Karakorum, Pakistan), Geol. Rundsch., 85, 683–704, 1996.

Gansser, A.: The significance of the Himalayan suture zone, Tectonophysics, 62, 37–52, 1980.

Gao, G., Kang, G., Li, G., Bai, C., and Wu, Y.: An analysis of crustal magnetic anomaly and Curie surface in west Himalayan syntaxis and adjacent area, Acta Geod. Geophys., 52, 407–420, 2017.

Gnojek, I., Sedlak, J., Rapprich, V., Skacelova, Z., Mlcoch, B., Krentz, O., and Casar-Garcia, R.: Structure of the Carboniferous Altenberg-Teplice Caldera (Eastern part of the Krusne hory/Erzgebirge Mts.) revealed by combined airborne and ground gamma-ray spectrometry, J. Geosci., 63, 3–20, 2018.

Goes, S., Hasterok, D., Schutt, D. L., and Klöcking, M.: Continental lithospheric temperatures: A review, Phys. Earth Planet. Inter., 306, 106509, 2020.

Grujic, D., Warren, C. J., and Wooden, J. L.: Rapid synconvergent exhumation of Miocene-aged lower orogenic crust in the eastern Himalaya, Lithosphere, 3, 346–366, 2011.

Guerra, I., Luongo, G., Maistrello, M., and Scarascia, S.: Deep seismic sounding along the profile Lawrencepur-Sango Sar (Nanga Parbat), Bull. Geofis. Teor. Appl., 25, 211–219, 1983.

Guevara, V.E., Smye, A.J., Caddick, M.J., Searle, M.P., Olsen, T., Whalen, L., Kylander-Clark, A.R., Jercinovic, M.J. and Waters, D.J.: A modern pulse of ultrafast exhumation and diachronous crustal melting in the Nanga Parbat Massif. Science Advances, 8(31), 2022.

Hacker, B. R., Kelemen, P. B., and Behn, M. D.: Continental Lower Crust, Annu. Rev. Earth Planet. Sci., 43, 167–205, 2015.

Hasterok, D., and Chapman, D. S.: Heat production and geotherms for the continental lithosphere, Earth Planet. Sci. Lett., 307, 59–70, 2011.

Hasterok, D., Gard, M., and Webb, J.: On the radiogenic heat production of metamorphic, igneous, and sedimentary rocks, Geosci. Front., 9, 1777–1794, 2018.

Hazarika, D., Sen, K., and Kumar, N.: Characterizing the intracrustal low velocity zone beneath northwest India–Asia collision zone, Geophys. J. Int., 199, 1338–1353, 2014.

Hillis, R., Hand, M., Mildren, S., Reid, P., Reynolds, S., and Nelson, E.: Hot dry rock geothermal exploration in Australia, ASEG Ext. Abstr., 2004, 1–4, 2004.

Hindle, D., and Besson, O.: A corrected finite-difference scheme for the flexure equation with abrupt changes in coefficient, Solid Earth, 14, 197–212, 2023.

Jadoon, I. A. K., Ding, L., Jadoon, S.-R. K., Bhatti, Z. I., Shah, S. T. H., and Qasim, M.: Lithospheric Deformation and Active Tectonics of the NW Himalayas, Hindukush, and Tibet, Lithosphere, 2021, 7866954, 2021.

Jagoutz, O., and Schmidt, M. W.: The formation and bulk composition of modern juvenile continental crust: The Kohistan arc, Chem. Geol., 298, 79–96, 2012.

Jamieson, R. A., and Beaumont, C.: Coeval thrusting and extension during lower crustal ductile flow – implications for exhumation of high-grade metamorphic rocks, J. Metamorph. Geol., 29, 33–51, 2011.

Jamieson, R. A., Beaumont, C., Nguyen, M. H., and Lee, B.: Interaction of metamorphism, deformation and exhumation in large convergent orogens, J. Metamorph. Geol., 20, 9–24, 2002.

Jaupart, C., and Mareschal, J. C.: Constraints on crustal heat production from heat flow data, in: The Crust (Rudnick R. L. Ed.), Treatise on Geochemistry, Vol. 3, Elsevier-Pergamon, 65–84, 2005.

Jaupart, C., Mareschal, J.-C., and Iarotsky, L.: Radiogenic heat production in the continental crust, Lithos, 262, 398–427, 2016.

Kazmi, A. H., Lawrance, R. D., Dawood, H., Snee, L. W., and Hussain, S. S.: Geology of The Indus Suture Zone In The Mingora-Swat Shangla Area Of Swat, N. Pakistan, J. Himal. Earth Sci., 17, 1984.

Kind, R., and Yuan, X.: Seismic Images of the Biggest Crash on Earth, Science, 329, 1479–1480, 2010.

Koltzer, N., Scheck-Wenderoth, M., Bott, J., Cacace, M., Frick, M., Sass, I., Fritsche, J.-G., and Bär, K.: The effects of regional fluid flow on deep temperatures (Hesse, Germany), Energies, 12, 2081, 2019.

Kufner, S.-K., Schurr, B., Sippl, C., Yuan, X., Ratschbacher, L., Ischuk, A., Murodkulov, S., Schneider, F., Mechie, J., and Tilmann, F.: Deep India meets deep Asia: Lithospheric indentation, delamination and break-off under Pamir and Hindu Kush (Central Asia), Earth Planet. Sci. Lett., 435, 171–184, 2016.

Kumar, N., Aoudia, A., Guidarelli, M., Babu, V. G., Hazarika, D., and Yadav, D. K.: Delineation of lithosphere structure and characterization of the Moho geometry under the Himalaya–Karakoram–Tibet collision zone using surface-wave tomography, Geol. Soc. Lond. Spec. Publ., 481, 19–40, 2019.

Kumar, P. S., Menon, R., and Reddy, G. K.: The role of radiogenic heat production in the thermal evolution of a Proterozoic granulite-facies orogenic belt: Eastern Ghats, Indian Shield, Earth Planet. Sci. Lett., 254, 39–54, 2007.

Kumar, P. S., Menon, R., and Reddy, G. K.: Heat production heterogeneity of the Indian crust beneath the Himalaya: Insights from the northern Indian Shield, Earth Planet. Sci. Lett., 283, 190–196, 2009.

Kumar, V., Rai, S. S., Hawkins, R., and Bodin, T.: Seismic Imaging of Crust Beneath the Western Tibet-Pamir and Western Himalaya Using Ambient Noise and Earthquake Data, J. Geophys. Res. Solid Earth, 127, e2021JB022574, 2022.

Li, A., and Mashele, B.: Crustal structure in the Pakistan Himalaya from teleseismic receiver functions, Geochem. Geophys. Geosyst., 10, 2009.

Li, W., Chen, Y., Yuan, X., Schurr, B., Mechie, J., Oimahmadov, I., and Fu, B.: Continental lithospheric subduction and intermediate-depth seismicity: Constraints from S-wave velocity structures in the Pamir and Hindu Kush, Earth Planet. Sci. Lett., 482, 478–489, 2018.

Malinconico, L. L.: The structure of the Kohistan-arc terrane in northern Pakistan as inferred from gravity data, Tectonophysics, 124, 297–307, 1986.

McCay, A. T., and Younger, P. L.: Ranking the geothermal potential of radiothermal granites in Scotland: Are any others as hot as the Cairngorms?, Scott. J. Geol., 53, 1–11, 2017.

McKenzie, D., Jackson, J., and Priestley, K.: Thermal structure of oceanic and continental lithosphere, Earth Planet. Sci. Lett., 233, 337–349, 2005.

McKenzie, D., and Priestley, K.: Speculations on the formation of cratons and cratonic basins, Earth Planet. Sci. Lett., 435, 94–104, 2016.

Mechie, J., Yuan, X., Schurr, B., Schneider, F., Sippl, C., Ratschbacher, L., Minaev, V., Gadoev, M., Oimahmadov, I., and Abdybachaev, U.: Crustal and uppermost mantle velocity structure along a profile across the Pamir and southern Tien Shan as derived from project TIPAGE wide-angle seismic data, Geophys. J. Int., 188, 385–407, 2012.

Moeck, I. S.: Catalog of geothermal play types based on geologic controls, Renew. Sust. Energ. Rev., 37, 867–882, 2014.

Muhammad, S., and Haq, A.: Spatial distribution of radon contamination in hot springs water and its cancer and non-cancer risks in the Hunza-Nagar valley, Pakistan, Environ. Geochem. Health, 45, 5829–5840, 2023.

Palin, R. M., Searle, M. P., Waters, D. J., Horstwood, M. S. A., and Parrish, R. R.: Combined thermobarometry and geochronology of peraluminous metapelites from the Karakoram metamorphic complex, North Pakistan; New insight into the tectonothermal evolution of the Baltoro and Hunza Valley regions, J. Metamorph. Geol., 30, 793–820, 2012.

Perry, H. K. C., Jaupart, C., Mareschal, J.-C., and Bienfait, G.: Crustal heat production in the Superior Province, Canadian Shield, and in North America inferred from heat flow data, J. Geophys. Res. Solid Earth, 111, 2005JB003893, 2006.

Petterson, M. G.: A review of the geology and tectonics of the Kohistan island arc, north Pakistan, Geol. Soc. Lond. Spec. Publ., 338, 287–327, 2010.

Petterson, M. G.: The plutonic crust of Kohistan and volcanic crust of Kohistan–Ladakh, north Pakistan/India: Lessons learned for deep and shallow arc processes, Geol. Soc. Lond. Spec. Publ., 483, 123–164, 2019.

Petterson, M. G., Crawford, M. B., and Windley, B. F.: Petrogenetic implications of neodymium isotope data from the Kohistan batholith, North Pakistan, J. Geol. Soc., 150, 125–129, 1993.

Podugu, N., Ray, L., Singh, S. P., and Roy, S.: Heat flow, heat production, and crustal temperatures in the Archaean Bundelkhand craton, north-central India: Implications for thermal regime beneath the Indian shield, J. Geophys. Res. Solid Earth, 122, 5766–5788, 2017.

Priestley, K., Ho, T., and Mitra, S.: The crustal structure of the Himalaya: A synthesis, Geol. Soc. Lond. Spec. Publ., 483, 483–516, 2019.

Priestley, K., Jackson, J., and McKenzie, D.: Lithospheric structure and deep earthquakes beneath India, the Himalaya and southern Tibet, Geophys. J. Int., 172, 345–362, 2008.

Rai, S. S., Priestley, K., Gaur, V. K., Mitra, S., Singh, M. P., and Searle, M.: Configuration of the Indian Moho beneath the NW Himalaya and Ladakh, Geophys. Res. Lett., 33, 2006GL026076, 2006.

Razi, A. S., Levin, V., Roecker, S. W., and Huang, G. D.: Crustal and uppermost mantle structure beneath western Tibet using seismic traveltime tomography, Geochem. Geophys. Geosyst., 15, 434–452, 2014.

Roy, S., and Mareschal, J.-C.: Constraints on the deep thermal structure of the Dharwar craton, India, from heat flow, shear wave velocities, and mantle xenoliths, J. Geophys. Res., 116, B02409, 2011.

Rudnick, R. L., and Gao, S.: Vol. 3: The Crust, 3.01–The Composition of the Continental Crust, Treatise on Geochemistry, 1–64, 2003.

Schneider, F. M., Yuan, X., Schurr, B., Mechie, J., Sippl, C., Kufner, S.-K., Ratschbacher, L., Tilmann, F., Oimahmadov, I., Gadoev, M., Minaev, V., Abdybachaev, U., Orunbaev, S., Ischuk, A., and Murodkulov, S.: The Crust in the Pamir: Insights From Receiver Functions, J. Geophys. Res. Solid Earth, 124, 9313–9331, 2019.

Searle, M. P., and Hacker, B. R.: Structural and metamorphic evolution of the Karakoram and Pamir following India–Kohistan–Asia collision, Geol. Soc. Lond. Spec. Publ., 483, 555–582, 2019.

Searle, M. P., and Khan, M. A.: Geological map of north Pakistan and adjacent areas of northern Ladakh and western Tibet (Western Himalaya, Salt Ranges, Kohistan, Karakoram, Hindu Kush) [Map], Oxford University, 1996.

Searle, M. P., Parrish, R. R., Thow, A. V., Noble, S. R., Phillips, R. J., and Waters, D. J.: Anatomy, age and evolution of a collisional mountain belt: The Baltoro granite batholith and Karakoram Metamorphic Complex, Pakistani Karakoram, J. Geol. Soc., 167, 183–202, 2010.

Searle, M. P., Rex, A. J., Tirrul, R., Rex, D. C., Barnicoat, A., and Windley, B. F.: Metamorphic, magmatic, and tectonic evolution of the central Karakoram in the Biafo-Baltoro-Hushe regions of northern Pakistan, in: Tectonics of the western Himalayas, Vol. 232, Geological Society of America, 1989.

Searle, M. P., and Tirrul, R.: Structural and thermal evolution of the Karakoram crust, J. Geol. Soc., 148, 65–82, 1991.

Shanker, R.: Heat-flow map of India and discussions on its geological and economic significance, Indian Minerals, 42, 89–110, 1988.

Shuja, T. A.: Geothermal areas in Pakistan, Geothermics, 15, 719–723, 1986.

Tahirkheli, R. K.: Geology of Kohistan and adjoining Eurasian and Indo-Pakistan continents, Pakistan, Geol. Bull. Univ. Peshawar, 11, 1–30, 1979.

Treloar, P. J., Brodie, K. H., Coward, M. P., Jan, M. Q., Khan, M. A., Knipe, R. J., Rex, D. C., and Williams, M. P.: The evolution of the Kamila shear zone, Kohistan, Pakistan, in: Exposed cross-sections of the continental crust, Vol. 317, Springer, 175–214, 1990.

Treloar, P. J., Petterson, M. G., Jan, M. Q., and Sullivan, M. A.: A re-evaluation of the stratigraphy and evolution of the Kohistan arc sequence, Pakistan Himalaya: Implications for magmatic and tectonic arc-building processes, J. Geol. Soc., 153, 681–693, 1996.

Vilà, M., Fernández, M., and Jiménez-Munt, I.: Radiogenic heat production variability of some common lithological groups and its significance to lithospheric thermal modeling, Tectonophysics, 490, 152–164, 2010.

Villa, I. M., Lemennicier, Y., and Le Fort, P.: Late Miocene to Early Pliocene tectonometamorphism and cooling in south-central Karakorum and Indus-Tsangpo suture, Chogo Lungma area (NE Pakistan), Tectonophysics, 260, 201–214, 1996.

Wang, Y., Zhou, L., and Zhao, L.: Cratonic reactivation and orogeny: An example from the northern margin of the North China Craton, Gondwana Res., 24, 1203–1222, 2013.

Wanner, C., Diamond, L. W., and Alt-Epping, P.: Quantification of 3-D Thermal Anomalies from Surface Observations of an Orogenic Geothermal System (Grimsel Pass, Swiss Alps), J. Geophys. Res. Solid Earth, 124, 10839–10854, 2019.

Wanner, C., Waber, H. N., and Bucher, K.: Geochemical evidence for regional and long-term topography-driven groundwater flow in an orogenic crystalline basement (Aar Massif, Switzerland), J. Hydrol., 581, 124374, 2020.

Warren, C. J., Grujic, D., Kellett, D. A., Cottle, J., Jamieson, R. A., and Ghalley, K. S.: Probing the depths of the India-Asia collision: U-Th-Pb monazite chronology of granulites from NW Bhutan, Tectonics, 30, 2010TC002738, 2011.

Weller, O. M., Jackson, S., Miller, W. G. R., St-Onge, M. R., and Rayner, N.: Quantitative elemental mapping of granulite-facies monazite: Textural insights and implications for petrochronology, J. Metamorph. Geol., 38, 853–880, 2020.

Whittington, A. G.: Exhumation overrated at Nanga Parbat, northern Pakistan, Tectonophysics, 260, 215–226, 1996.

Wittlinger, G., Farra, V., Hetényi, G., Vergne, J., and Nábělek, J.: Seismic velocities in Southern Tibet lower crust: A receiver function approach for eclogite detection, Geophys. J. Int., 177, 1037–1049, 2009.

Yakymchuk, C., and Brown, M.: Divergent behaviour of Th and U during anatexis: Implications for the thermal evolution of orogenic crust, J. Metamorph. Geol., 37, 899–916, 2019.

Zeitler, P. K.: Cooling history of the NW Himalaya, Pakistan, Tectonics, 4, 127–151, 1985.

Zeitler, P. K., Chamberlain, C. P., and Smith, H. A.: Synchronous anatexis, metamorphism, and rapid denudation at Nanga Parbat (Pakistan Himalaya), Geology, 21, 347–350, 1993.

Zhao, J., Yuan, X., Liu, H., Kumar, P., Pei, S., Kind, R., Zhang, Z., Teng, J., Ding, L., Gao, X., Xu, Q., and Wang, W.: The boundary between the Indian and Asian tectonic plates below Tibet, Proc. Natl. Acad. Sci. USA, 107, 11229–11233, 2010.